

A Simple Analytical Model of the Nocturnal Low-Level Jet over the Great Plains of the United States

YU DU

*Laboratory for Climate and Ocean-Atmosphere Studies, Department of Atmospheric and Oceanic Sciences,
School of Physics, Peking University, Beijing, China*

RICHARD ROTUNNO

National Center for Atmospheric Research, Boulder, Colorado*

(Manuscript received 11 March 2014, in final form 19 June 2014)

ABSTRACT

A simple analytical model including both diurnal thermal forcing over sloping terrain (the “Holton” mechanism) and diurnally varying boundary layer friction (the “Blackadar” mechanism) is developed to account for the observed amplitude and phase of the low-level jet (LLJ) over the Great Plains and to understand better the role of each mechanism. The present model indicates that, for the pure Holton mechanism (time-independent friction coefficient), the maximum southerly wind speed v_{\max} occurs (depending on the assumed friction coefficient) between sunset and midnight local standard time, which is earlier than the observed after-midnight maximum. For the pure Blackadar mechanism (time-independent thermal forcing), the present model shows that v_{\max} generally occurs later (closer to sunrise) than observed and has a strong latitudinal dependence. For both mechanisms combined, the present model indicates that v_{\max} occurs near to the observed time, which lies between the time obtained in the pure Holton mechanism and the time obtained in the pure Blackadar mechanism; furthermore, v_{\max} is larger (and closer to that observed) than in each one considered individually. The amplitude and phase of the LLJ as a function of latitude can be obtained by the combined model by allowing for the observed latitude-dependent mean and diurnally varying thermal forcing.

1. Introduction

The warm-season nocturnal low-level jet (LLJ) over the Great Plains of the United States (Great Plains) has been extensively studied over the past 60 years through observations (e.g., Bonner 1968; Whiteman et al. 1997; Mitchell et al. 1995; Banta et al. 2002), numerical simulations (e.g., Zhong et al. 1996; Jiang et al. 2007, hereinafter J07; Parish and Oolman 2010, hereinafter P10; Rife et al. 2010), and theoretical models (e.g., Blackadar 1957; Holton 1967; Shapiro and Fedorovich 2009). The LLJ is a feature of the boundary layer and is characterized by a pronounced diurnal cycle with the maximum at night. In

the present study, we develop a simple analytical model that accounts for the observed amplitude and phase of the LLJ as a function of latitude.

Two main popular theories have been proposed to explain the occurrence of the LLJ, one centered on the diurnal variation of boundary layer friction (Blackadar 1957) and the other focused on the diurnal heating of the east–west sloping terrain of the Great Plains (Holton 1967).

Blackadar (1957) proposed that the supergeostrophic LLJ frequently observed at night is a result of the inertial oscillation of the ageostrophic wind triggered by the sudden decay of eddy viscosity after sunset. During the daytime, turbulent vertical mixing associated with the heated ground results in the retardation of the wind to subgeostrophic values in the boundary layer. At sunset, when turbulent stresses shut down because of the rapid stabilization of the boundary layer, air parcels suddenly accelerate horizontally. Subsequently, the Coriolis force rotates this accelerating and frictionless ageostrophic wind and causes an inertial oscillation with supergeostrophic

*The National Center for Atmospheric Research is sponsored by the National Science Foundation.

Corresponding author address: Dr. Richard Rotunno, MMM Division, Earth System Laboratory, National Center for Atmospheric Research, P.O. Box 3000, Boulder, CO 80307-3000.
E-mail: rotunno@ucar.edu

winds being reached after several hours. Based on Blackadar's conceptual model, Shapiro and Fedorovich (2010) established an exact analytical one-dimensional model to describe the evolution of the nocturnal low-level jet after sunset. Their model takes the initial (sunset) value of the winds from a steady-state Ekman layer having a large eddy viscosity and solves for the subsequent evolution of the flow with a much smaller eddy viscosity typical of the night. Their solution suggests that more intense jets are related to larger reductions in eddy viscosity. Van de Wiel et al. (2010) extended Blackadar's concept to consider frictional effects within the nocturnal boundary layer and found that the oscillation of the wind speed profile is around the nocturnal equilibrium wind vector instead of the geostrophic wind vector. In these theories, the interest is confined to the development stage (after sunset) of the LLJ and the solutions do not apply past sunrise.

The theory proposed by Holton (1967) stressed the important role of thermal forcing in the diurnal oscillation of the boundary layer wind above sloping terrain. Holton (1967) derived viscous momentum and diabatic thermodynamic energy equations with time-independent eddy viscosity and heat conductivity, respectively, for a stably stratified sloping boundary layer and obtained diurnally periodic solutions for the wind oscillation. However, the results did not correctly predict the observed phase of the diurnal oscillations.

Since these two well-known theories alone could not adequately explain the observations, Bonner and Paegle (1970) represented diurnal thermal forcing over sloping terrain (the "Holton" mechanism) through a diurnally varying geostrophic wind in combination with a diurnally varying eddy viscosity (the "Blackadar" mechanism) and obtained a better reproduction of the observed LLJ over the Great Plains. They noted that the amplitude of the oscillation in their solution is fairly sensitive to the time-varying geostrophic wind and viscosity, but they did not discuss in detail the response to varying parameters for the two mechanisms and their relationship to each other. Paegle and Rasch (1973) further discussed the three-dimensional features of diurnally varying boundary layer flows using the combined model.

J07, using an atmospheric general circulation model (AGCM), found that the LLJ can be generated by either the Blackadar or the Holton¹ mechanism but that either mechanism alone produces an unrealistic timing of the

LLJ maximum and an incorrect dependence of this timing on latitude. P10, using an idealized model, argued that the Blackadar mechanism is mainly responsible for the nocturnal wind maxima, and that the sloping terrain plays a key role in the establishment of the mean flow but plays an adverse role in the nighttime maximum intensity of the LLJ. We note that the latter idealized model only includes a nighttime period and does not include the complete diurnal cycle of heating and cooling over sloping terrain.

Therefore, to reconcile some of the differing interpretations offered in the literature, it is desired to establish a simpler analytical model that spans the diurnal cycle and includes both diurnal thermal forcing over sloping terrain and diurnally varying eddy viscosity. Following the Bonner–Paegle approach, but representing vertical diffusion as a linear damping and dividing a day into only two periods with different friction coefficients, we obtained such a simpler model and its analytical solution. This solution allows for easier access to the factors underlying the diurnal variation of the LLJ, such as its dependence on latitude, frictional effects, and the mean and diurnal thermal forcing. This simple analytical model for the diurnal cycle of the LLJ is described in section 2. In section 3, we present solutions for three problems: the Holton mechanism (diurnal pressure gradient, time-independent friction coefficient), the Blackadar mechanism (time-independent pressure gradient, diurnally varying friction coefficient), and their combination. We also examine the sensitivity of the amplitude and phase of the LLJ oscillation to different parameters in our model. In section 4, we compare the results from our model to an analysis of the LLJ from the North American Regional Reanalysis (NARR) (Mesinger et al. 2006) and in particular discuss the meridional variation of the LLJ over the Great Plains.

2. Description of a simple analytical linear model

a. Equations of motion

We consider the one-dimensional linear equations of motion for frictional flow on an f plane:

$$\frac{\partial u}{\partial t} - fv = -\frac{1}{\rho} \frac{\partial P}{\partial x} - \alpha u, \quad (2.1)$$

$$\frac{\partial v}{\partial t} + fu = -\alpha v, \quad (2.2)$$

$$-\frac{1}{\rho} \frac{\partial P}{\partial x} = \bar{F} + \hat{F} \cos \omega t, \quad (2.3)$$

where (u, v) are the wind components in the (x, y) directions, respectively; $\alpha(t)$ is the diurnally varying

¹ The Holton mechanism was simplified in the studies of Bonner and Paegle (1970) and Paegle and Rasch (1973) by accounting for the heated slope only through the diurnal variation of the pressure gradient. This usage is now common.

frictional coefficient; P is the pressure; ρ is the density of air; f is the Coriolis parameter; and ω is the diurnal frequency ($=2\pi \text{ day}^{-1}$). Following [Haurwitz \(1947\)](#) and [Schmidt \(1947\)](#) in their classic studies of the sea breeze, the frictional force (per unit mass) has been simplified to $(-\alpha u, -\alpha v)$. The pressure gradient force (per unit mass) in the x direction is composed of a mean (\bar{F}) and a diurnally varying ($\hat{F} \cos \omega t$) contribution. The diurnally varying part of the pressure gradient is associated with the diurnally varying east–west temperature difference over the sloping terrain of the Great Plains; the pressure gradient in the y direction is neglected in the present study (as in [P10](#)). A recent paper by [Pu and Dickinson \(2014\)](#) includes this effect and is briefly discussed in the summary.

b. Nondimensional equations

It is convenient to nondimensionalize variables as

$$U = \tilde{u} + i\tilde{v}, \quad (\tilde{u}, \tilde{v}) = (u, v) \left(\frac{\omega}{|\bar{F}| + |\hat{F}|} \right),$$

$$b = \frac{\alpha}{\omega}, \quad a = \frac{f}{\omega}, \quad \tau = \omega t,$$

$$\bar{\varepsilon} = \frac{\bar{F}}{|\bar{F}| + |\hat{F}|}, \quad \hat{\varepsilon} = \frac{\hat{F}}{|\bar{F}| + |\hat{F}|}.$$

With these definitions and [\(2.3\)](#), [\(2.1\)](#) and [\(2.2\)](#) reduce to the single complex nondimensional equation

$$\frac{dU}{d\tau} + (b + ia)U = (\bar{\varepsilon} + \hat{\varepsilon} \cos \tau, 0). \quad (2.4)$$

The physical meaning of the above-mentioned nondimensional parameters in [\(2.4\)](#) is given in [Table 1](#).

Considering the significant difference of eddy viscosity between daytime and nighttime, we set

$$b = \begin{cases} b_1 & \text{for } n\pi \leq \tau \leq (n+1)\pi \\ b_2 & \text{for } (n+1)\pi \leq \tau \leq (n+2)\pi \end{cases},$$

$$n = 0, 2, 4, 6, \dots,$$

where $\tau = (n+1)\pi$ is considered to be sunset (1800 LST) when the diurnal pressure gradient force ($\hat{\varepsilon} \cos \tau$) reaches its (negative) minimum value.²

c. Analytical solutions

The periodic solutions to [\(2.4\)](#) are similarly divided into daytime and nighttime intervals,

TABLE 1. Nondimensional parameters for the linear model.

Control parameter	Description
\tilde{u}	Nondimensional wind component in x direction $u\omega/(\bar{F} + \hat{F})$
\tilde{v}	Nondimensional wind component in y direction $v\omega/(\bar{F} + \hat{F})$
τ	Nondimensional time ωt
a	Ratio of inertial to diurnal frequency f/ω
b	Ratio of friction coefficient to diurnal frequency α/ω
$\bar{\varepsilon}$	Nondimensional mean east–west pressure gradient $\bar{F}/(\bar{F} + \hat{F})$
$\hat{\varepsilon}$	Nondimensional amplitude of diurnal east–west pressure gradient $\hat{F}/(\bar{F} + \hat{F})$

$$U = \begin{cases} U_1 & \text{for } n\pi \leq \tau \leq (n+1)\pi \\ U_2 & \text{for } (n+1)\pi \leq \tau \leq (n+2)\pi \end{cases},$$

$$n = 0, 2, 4, 6, \dots$$

Continuity of the velocity at sunrise and sunset requires that

$$U_1(n\pi) = U_2(n\pi + 2\pi) \quad (2.5)$$

and

$$U_1(n\pi + \pi) = U_2(n\pi + \pi); \quad (2.6)$$

the solution of [\(2.4\)](#) is

$$U_{1,2} = U_{\text{Forced}_{1,2}} + U_{\text{Free}_{1,2}}, \quad (2.7)$$

where

$$U_{\text{Forced}_{1,2}}(\tau) = \frac{\bar{\varepsilon}}{b_{1,2} + ia} + \frac{\hat{\varepsilon}}{2} \left[\frac{e^{i\tau}}{b_{1,2} + i(a+1)} + \frac{e^{-i\tau}}{b_{1,2} + i(a-1)} \right] \quad (2.8)$$

and

$$U_{\text{Free}_{1,2}}(\tau) = C_1 e^{-(b_1 + ia)(\tau - n\pi)}, \quad C_2 e^{-(b_2 + ia)(\tau - n\pi - \pi)}. \quad (2.9)$$

Applying the conditions [\(2.5\)](#) and [\(2.6\)](#), we have

$$U_{\text{Forced}_1}(n\pi) + C_1 = U_{\text{Forced}_2}[(n+2)\pi] + C_2 e^{-(b_2 + ia)\pi} \quad (2.10)$$

² Sunset in summer is at about 2000 LST. However, 1800 LST is reasonable for the (negative) minimum pressure gradient force.

and

$$U_{\text{Forced}_1}[(n+1)\pi] + C_1 e^{-(b_1+ia)\pi} = U_{\text{Forced}_2}[(n+1)\pi] + C_2. \quad (2.11)$$

Using (2.8) and solving for the unknown constants gives

$$C_1 = \frac{\bar{E}[1 - e^{-(b_2+ia)\pi}] + \hat{E}[1 + e^{-(b_2+ia)\pi}]}{1 - e^{-(b_1+b_2+2ia)\pi}} \quad (2.12)$$

and

$$C_2 = \frac{-\bar{E}[1 - e^{-(b_1+ia)\pi}] + \hat{E}[1 + e^{-(b_1+ia)\pi}]}{1 - e^{-(b_1+b_2+2ia)\pi}}, \quad (2.13)$$

where

$$\hat{E} = \frac{\hat{\varepsilon}}{2} \left[\frac{1}{b_2 + i(a+1)} + \frac{1}{b_2 + i(a-1)} - \frac{1}{b_1 + i(a+1)} - \frac{1}{b_1 + i(a-1)} \right] \quad (2.14)$$

and

$$\bar{E} = \bar{\varepsilon} \left(\frac{1}{b_2 + ia} - \frac{1}{b_1 + ia} \right). \quad (2.15)$$

The solution is therefore

$$U_1(\tau) = U_{\text{Forced}_1}(\tau) + C_1 e^{-(b_1+ia)(\tau-n\pi)} \quad (2.16)$$

and

$$U_2(\tau) = U_{\text{Forced}_2}(\tau) + C_2 e^{-(b_2+ia)(\tau-n\pi-\pi)} \quad (2.17)$$

with the definitions (2.8), (2.12), and (2.13).

3. Discussion of the analytical solution

The analytical solution of the present simple model is used to discuss three problems: the Holton mechanism (diurnal pressure gradient, time-independent friction coefficient), the Blackadar mechanism (time-independent pressure gradient, diurnally varying friction coefficient), and their combination.

a. Problem 1: The Holton mechanism

Since Holton (1967) described the nature of the LLJ as a response to the diurnal heating and cooling of sloping terrain with constant viscosity in time, we set $b_1 = b_2 = b_0$ in (2.16) and (2.17) for this problem. The solutions (2.16) and (2.17) reduce to

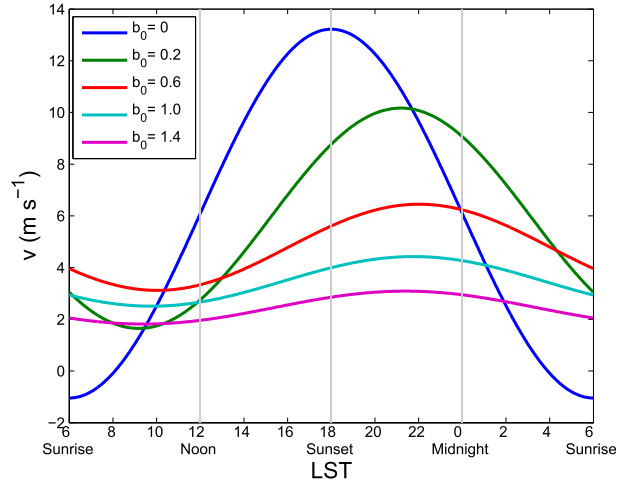


FIG. 1. The diurnal variations of v with different b_0 values for the Holton mechanism. The setting of the parameters is $\bar{F} \cong -5.8 \times 10^{-4} \text{ m s}^{-2}$, $\hat{F} \cong 1.7 \times 10^{-4} \text{ m s}^{-2}$, and $a = f/\omega = 1.15$ (latitude 35°N).

$$U(\tau) = \frac{\bar{\varepsilon}}{b_0 + ia} + \frac{\hat{\varepsilon}}{2} \left[\frac{e^{i\tau}}{b_0 + i(a+1)} + \frac{e^{-i\tau}}{b_0 + i(a-1)} \right] \quad \text{for}$$

$$n\pi \leq \tau \leq (n+2)\pi. \quad (3.1)$$

The solution here is a combination of steady Ekman balance (first term on the rhs) plus the time variation forced at the diurnal frequency; that is, there are no inertial oscillations. By the definitions given above, we have

$$\tilde{u} = \frac{\bar{\varepsilon}b_0}{b_0^2 + a^2} + \hat{\varepsilon} \sqrt{\frac{b_0^2 + 1}{(a^2 + b_0^2 - 1)^2 + 4b_0^2}} \cos(\tau - \phi), \quad (3.2)$$

where $\phi = \tan^{-1}[(-a^2 + b_0^2 + 1)/b_0(a^2 + b_0^2 + 1)]$ and

$$\tilde{v} = -\frac{\bar{\varepsilon}a}{b_0^2 + a^2} - \frac{\hat{\varepsilon}a}{\sqrt{(a^2 + b_0^2 - 1)^2 + 4b_0^2}} \sin(\tau + \psi), \quad (3.3)$$

where $\psi = \tan^{-1}[(a^2 + b_0^2 - 1)/2b_0]$.

Based on the time-mean geostrophic wind $\bar{v}_g \sim 7 \text{ m s}^{-1}$ and the amplitude of the diurnally varying geostrophic wind $\hat{v}_g \sim 2 \text{ m s}^{-1}$ at a latitude of approximately 35°N (Fig. 3b of P10), we estimate $\bar{F} \cong -7 \text{ m s}^{-1} \times (8.3 \times 10^{-5} \text{ s}^{-1}) \cong -5.8 \times 10^{-4} \text{ m s}^{-2}$ and similarly $\hat{F} \cong 1.7 \times 10^{-4} \text{ m s}^{-2}$ ($\bar{\varepsilon} = -7/9$, $\hat{\varepsilon} = 2/9$) to obtain dimensional velocities and consider the case $a = f/\omega = 1.15$. Figure 1 shows the diurnal variations of v with different friction

coefficients b_0 from the analytical solution [(3.3)]. Inspection of the phase function $\psi(a, b_0)$ in (3.3) indicates that the maximum v (v_{\max}) occurs at sunset for either very small or very large friction coefficients; however, at intermediate values of b_0 , it can be shown that v_{\max} occurs much later. The latest time can be found by setting $\partial\psi/\partial b_0 = 0$, which gives $b_0 = \sqrt{a^2 - 1} \approx 0.6$ for the case illustrated in Fig. 1. Hence, the latest time for the jet-speed maximum (~ 2300 LST) is earlier than the observed maximum (~ 0100 LST; P10; J07). This result of our simple model is consistent with the statement in Holton (1967) that the phase of the observed oscillation lags the phase of that from his model by 2 or 3 h. The present 1D model derives from original studies of the sea breeze by Haurwitz (1947) and Schmidt (1947). In those studies the along-coast flow is found to be at its maximum (in midlatitudes) when the imposed diurnally varying cross-coast pressure gradient force is at its (negative) minimum (at sunset); friction was found to postpone the maximum until after sunset, consistent with the present results.

b. Problem 2: The Blackadar mechanism

Blackadar (1957) proposed that nocturnal supergeostrophic winds are due to an inertial oscillation induced by the reduction in eddy viscosity at sunset without considering the diurnal thermal effect. To represent this mechanism, we set $\hat{\epsilon} = 0$ in (2.16) and (2.17) for the Blackadar problem. The solutions (2.16) and (2.17) reduce to

$$U_1(\tau) = \bar{\epsilon} \left[\frac{1}{b_1 + ia} + \left(\frac{1}{b_2 + ia} - \frac{1}{b_1 + ia} \right) \times \frac{1 - e^{-(b_2 + ia)\pi}}{1 - e^{-(b_1 + b_2 + 2ia)\pi}} e^{-(b_1 + ia)(\tau - n\pi)} \right] \text{ for } n\pi \leq \tau \leq (n + 1)\pi \tag{3.4}$$

and

$$U_2(\tau) = \bar{\epsilon} \left[\frac{1}{b_2 + ia} - \left(\frac{1}{b_2 + ia} - \frac{1}{b_1 + ia} \right) \times \frac{1 - e^{-(b_1 + ia)\pi}}{1 - e^{-(b_1 + b_2 + 2ia)\pi}} e^{-(b_2 + ia)[\tau - (n + 1)\pi]} \right] \text{ for } (n + 1)\pi \leq \tau \leq (n + 2)\pi. \tag{3.5}$$

The solution here is composed of the steady Ekman solution (first terms on the rhs) plus the inertial oscillation

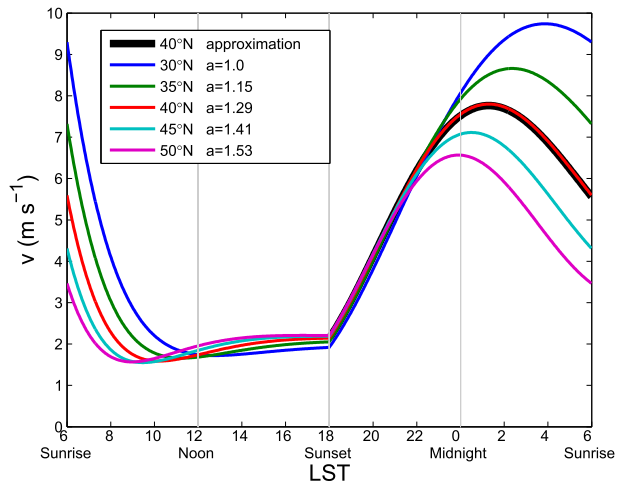


FIG. 2. The diurnal variations of v at different latitudes for the Blackadar mechanism. The setting of the parameters is $\bar{F} \cong -5.8 \times 10^{-4} \text{ m s}^{-2}$, $b_1 = 1.6$, and $b_2 = 0.2$. The thick black curve for 40°N shows the approximation (3.7) for the nighttime.

and frictional damping as a result of the transitions from daytime to nighttime Ekman solutions.

Based on the magnitude of the vertical diffusion coefficient ($K \approx 1 \text{ m}^2 \text{ s}^{-1}$ at nighttime and $K \approx 120 \text{ m}^2 \text{ s}^{-1}$ during the daytime from Fig. 7 of J07), we set $b_1 = \alpha/\omega = (K\partial^2/\partial z^2)/\omega = (K/\delta^2)/\omega = [(120 \text{ m}^2 \text{ s}^{-1})/(1 \text{ km})^2]/(7.26 \times 10^{-5} \text{ s}^{-1}) \approx 1.6$ and $b_2 = [(1 \text{ m}^2 \text{ s}^{-1})/(0.25 \text{ km})^2]/(7.26 \times 10^{-5} \text{ s}^{-1}) \approx 0.2$, where the boundary layer height scale δ is 1 km during the daytime and 0.25 km at night.

For $b_1 \sim O(1)$, the ratio $[1 - e^{-(b_1 + ia)\pi}]/[1 - e^{-(b_1 + b_2 + 2ia)\pi}] \approx 1$ and therefore (3.5) can be simplified to

$$\tilde{u}_2 \cong \bar{\epsilon} \left[\frac{b_2}{b_2^2 + a^2} + D \sin(a\tau' + \theta) \right] \tag{3.6}$$

and

$$\tilde{v}_2 \cong \bar{\epsilon} \left[-\frac{a}{b_2^2 + a^2} + D \cos(a\tau' + \theta) \right], \tag{3.7}$$

where $D = (b_1 - b_2)e^{-b_2\tau'}/\sqrt{(b_1^2 + a^2)(b_2^2 + a^2)}$, $\theta = \tan^{-1}[(a^2 - b_1b_2)/a(b_1 + b_2)]$, and $\tau' = \tau - (n + 1)\pi$.

Inspection of (3.6) and (3.7) reveals several important features of the solution. First, the amplitude of the inertial oscillation D is proportional to the day–night difference in friction coefficients ($b_1 - b_2$) and inversely proportional to the latitude parameter a . Second, the period of the oscillation is inversely proportional to a . Figure 2 shows $v(t; a)$ from (3.4) and (3.5); inspection of the solution in the sunset-to-sunrise interval shows that the solution is characterized by an inertial oscillation of decreasing period and amplitude with increasing latitude as expected from

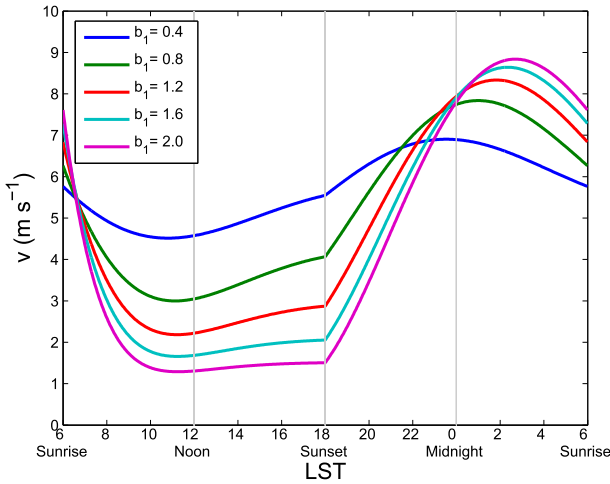


FIG. 3. The diurnal variations of v with different b_1 values at 35°N for the Blackadar mechanism. The setting of the parameters is $\bar{F} \cong -5.8 \times 10^{-4} \text{ m s}^{-2}$, $a = f/\omega = 1.15$ (latitude 35°N), and $b_2 = 0.2$.

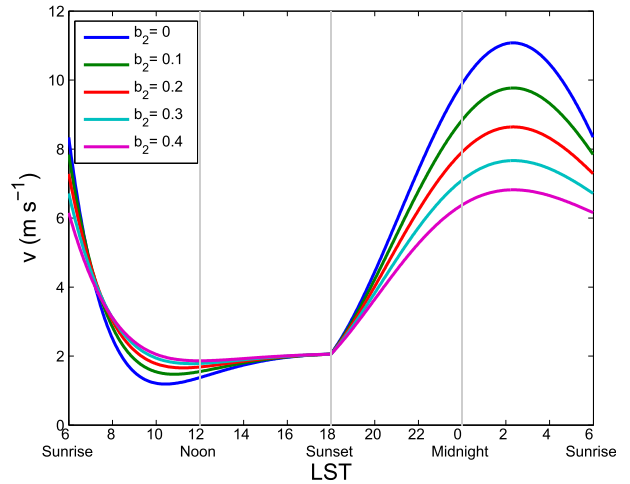


FIG. 4. The diurnal variations of v with different b_2 values at 35°N for the Blackadar mechanism. The setting of the parameters is $\bar{F} \cong -5.8 \times 10^{-4} \text{ m s}^{-2}$, $a = f/\omega = 1.15$ (latitude 35°N), and $b_1 = 1.6$.

(3.7). The approximated 40°N curve (3.7) in Fig. 2 (thick black line) shows that the approximation leading to (3.7) is excellent. The approximation (3.7) is similarly good at the other latitudes (not shown).

Figure 3 shows that the timing and amplitude of v_{max} is sensitive to the daytime friction coefficient b_1 (for fixed b_2), whereas Fig. 4 shows that it is primarily the amplitude of v_{max} that is sensitive to nighttime friction coefficient b_2 . Considering the limiting case over the Great Plains in which $b_2 \ll b_1 \sim a \sim O(1)$, (3.7) further reduces to

$$v(\tau') \approx -\frac{\bar{\epsilon}}{a} \left[1 - \frac{b_1}{\sqrt{b_1^2 + a^2}} e^{-b_2 \tau'} \cos(a\tau' + \theta) \right];$$

$$\theta = \tan^{-1}\left(\frac{a}{b_1}\right). \tag{3.8}$$

Equation (3.8) indicates that the maximum amplitude of the southerly flow and its latest time occur for the largest b_1 , consistent with Fig. 3. It also shows that the amplitude of the nighttime peak wind is exponentially damped by b_2 without changing its timing, consistent with Fig. 4.

The original Blackadar model (and its descendants) considers an initial-value problem, with the initial (sunset) ageostrophic velocity given, the geostrophic velocity fixed in time, and no frictional effects. The frictional effects are assumed to have taken place in the daytime and acted to produce a large ageostrophic imbalance that, upon the reduction of the frictional effects at sunset, is free to evolve. In diurnally periodic solutions, such as those presented here, the ageostrophic velocity at sunset is part of the solution; the geostrophic velocity and friction coefficients (b_1 , b_2) are given. In the present Blackadar case ($b_1 > b_2$), the geostrophic wind is constant; however, the

change in friction coefficient between day and night gives different daytime and nighttime Ekman solutions; the difference between these Ekman solutions, embodied in (2.15), sets the ageostrophic wind at sunset.

To illustrate the latter point, Fig. 3 shows that from approximately noon to sunset, the solution is nearly steady for a large b_1 , as can be seen by the exponential-decay term that multiplies the oscillatory part of the daytime solution [(3.4)]. This interval of a nearly steady solution is consistent with the study by Shapiro and Fedorovich (2010) in which the initial velocities for the nighttime solution are taken from assumed steady-state daytime values.

c. Problem 3: Combination of the Holton and Blackadar mechanisms

In this problem, we consider both the Blackadar and Holton mechanisms together [(2.16) and (2.17)]. Figure 5 shows that v_{max} occurs around 0100 LST, which is between the time obtained in the pure Holton mechanism (~ 2200 LST) and the time obtained in the pure Blackadar mechanism (~ 0300 LST); furthermore, the magnitude of v_{max} is larger in the combined case (and closer to observed values; see below) than in either one individually. With diurnally varying viscosity and diurnal thermal forcing, both the phase and magnitude of the LLJ are more similar to the LLJ from previous studies (e.g., J07; P10) or NARR data (Fig. 7) than with either mechanism in isolation.

4. Latitudinal variation of the LLJ

The long-term (1979–2001) summertime (June–August) NARR with high spatial (32-km horizontal grid, 45 layers) and temporal (3 hourly) resolution (Mesinger

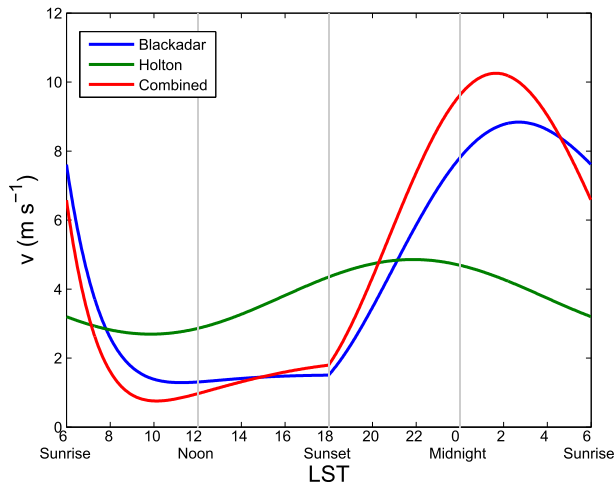


FIG. 5. Comparison of the diurnal variations of v among the Holton mechanism (green), the Blackadar mechanism (blue), and their combination (red). The setting of the parameters is $\bar{F} \cong -5.8 \times 10^{-4} \text{ m s}^{-2}$, $\hat{F} \cong 1.7 \times 10^{-4} \text{ m s}^{-2}$, $a = f/\omega = 1.15$ (latitude 35°N), $b_0 = 0.9$, $b_1 = 1.6$, and $b_2 = 0.2$.

et al. 2006) is used to analyze the climatological characteristics of the LLJ, including the latitudinal variation of its diurnal phase and amplitude. This dataset has been used in other similar studies (Pu and Dickinson 2014; J07) and has a longer period of record than any other analysis (e.g., the Rapid Update Cycle analysis). J07 found that

925 hPa was a good level for the NARR LLJ maximum (see Figs. 1b and 4a of J07). As shown in Fig. 6, a strong southerly wind at 925 hPa is located over the Great Plains. In the present study, we focus on the region $30^\circ\text{--}40^\circ\text{N}$, $95^\circ\text{--}100^\circ\text{W}$, shown by the box in Fig. 6. Figure 7 shows the latitudinal variation of the diurnal phase and amplitude for the meridional wind v in the analysis box. The southerly jet maximum v_{max} occurs around 0200 LST from 30°N to 40°N and its maximum amplitude is located at about 34°N , which is also consistent with the AGCM from the study of J07.

Next, we use our simple model to account for this observed amplitude and phase of the LLJ as a function of latitude.

First, we consider simple situations in which \bar{F} and \hat{F} are constant with latitude ($\bar{F} \cong -5.8 \times 10^{-4} \text{ m s}^{-2}$ and $\hat{F} \cong 1.7 \times 10^{-4} \text{ m s}^{-2}$). For the Blackadar solution, the time phase of the v_{max} (solid blue line in Fig. 8) exhibits a significant latitudinal shift; v_{max} occurs earlier at higher latitudes [because of the shorter inertial period ($2\pi/f$) as mentioned in section 3b]. Figure 9 (solid blue line) shows that v_{max} decreases with latitude. These features are generally consistent with Fig. 8c in J07. For the Holton solution, there is a weak temporal shift with a latitude of approximately 1 h in the time of v_{max} (solid black line in Fig. 8) compared to a corresponding approximately 2.5-h shift for the Blackadar solution, whereas the magnitude of

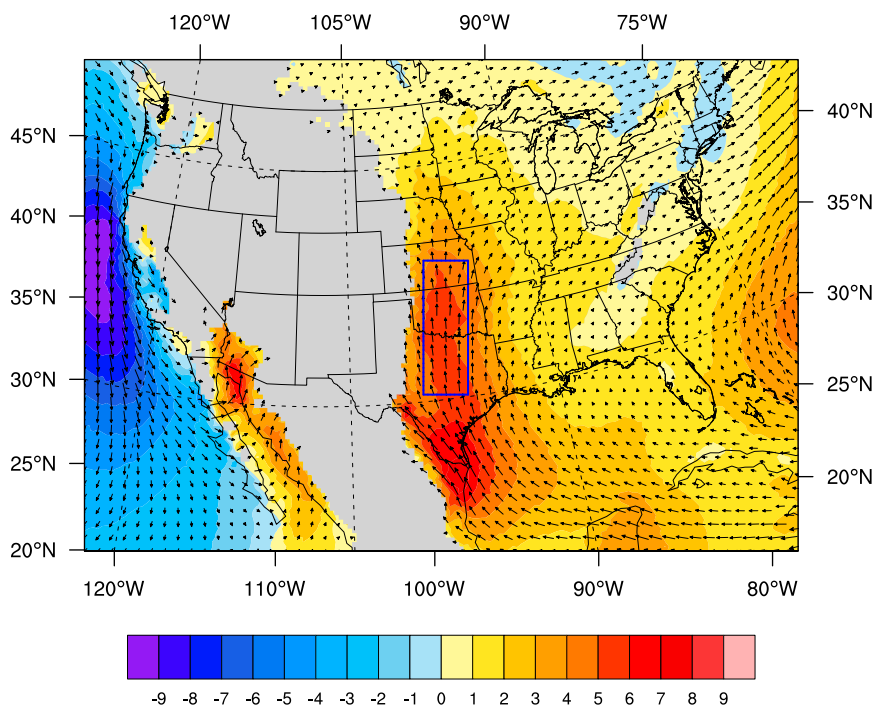


FIG. 6. Horizontal distribution of the averaged 925-hPa wind vectors and the meridional wind speed (shaded; m s^{-1}) from NARR during the summer (June–August) during 1979–2011. The blue rectangular box indicates the LLJ analysis box.

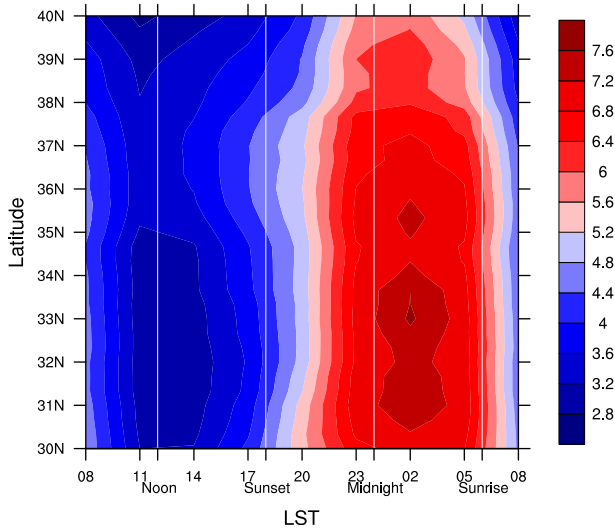


FIG. 7. Latitudinal variation of the diurnal variation of v at the 925-hPa level (shaded; m s^{-1}) (averaged along the x direction of the blue box in Fig. 6).

v_{max} (solid black line in Fig. 9) does not change with latitude. Note, however, that v_{max} decreases with latitude in the modeling of J07 (their Fig. 8b). In the combined solution (solid red line in Figs. 8 and 9), the time of v_{max} still exhibits a latitudinal shift and the magnitude decreases with latitude, which is not consistent with the NARR data (Fig. 7) and the results from J07.

To correctly reproduce the phase and qualitative changes of amplitude of the LLJ as a function of latitude, next we take into account the variation of \bar{F} and \hat{F} with latitude. Figure 10 shows the latitudinal variation of the daily-mean pressure gradient force ($g\partial Z_g/\partial x$, where Z_g is geopotential height) and the difference between the maximum and minimum pressure gradient forces in a day $[(g\partial Z_g/\partial x)_{\text{max}} - (g\partial Z_g/\partial x)_{\text{min}}]$ at the 925-hPa level averaged along the x axis of the blue box in Fig. 6 from the NARR data. As shown in Fig. 10, the NARR data during the summer season suggest that \bar{F} increases with latitude from 30° to 37°N and slightly decreases from 37° to 40°N , whereas \hat{F} decreases with latitude from 30° to 40°N . According to these variations, we let \bar{F} and \hat{F} vary with latitude in our model and obtain modified results in the Holton, Blackadar, and combined problems. For the Holton solution, v_{max} (dashed black line in Fig. 9) is essentially constant from 30° to 34°N and then decreases from 34° to 40°N because of decreasing \hat{F} , which is consistent with Fig. 8b of J07.

For the Holton or the Blackadar solutions considered individually, the latitudinal dependence of the time of v_{max} (dashed black and blue lines in Fig. 8) is independent of the latitudinal variation of \bar{F} and \hat{F} , because each solution has a distinct frequency (diurnal in Holton, Coriolis

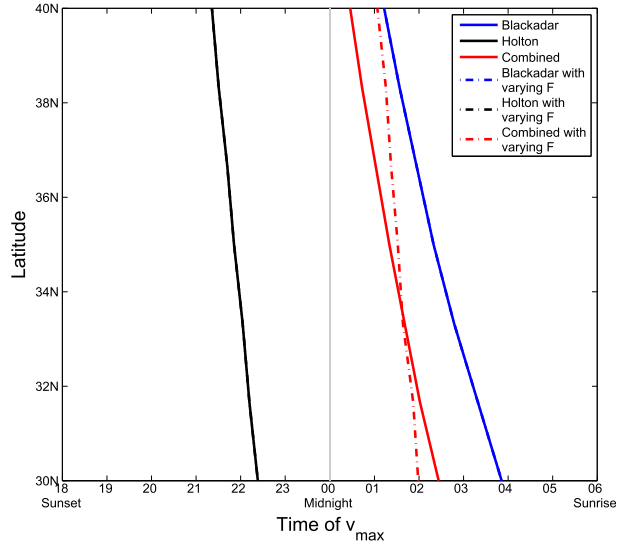


FIG. 8. Latitudinal variations of the time of v_{max} (averaged along the x direction of the blue box in Fig. 6) for the Blackadar mechanism (blue), the Holton mechanism (black), and their combination (red). Solid and dashed lines indicate constant and latitudinally varying F , respectively. Note that black and blue dashed lines are covered by the black and blue solid lines, respectively.

in Blackadar). However, in combination, the latitudinal dependence of the time of v_{max} (dashed red line in Fig. 8) changes and in fact is weaker (the maximum occurs at around 0200 LST) and v_{max} (dashed red line in Fig. 9) peaks near 34°N in the combined solution because of the coexistence of both diurnal and inertial time variations in (2.16) and (2.17). The features of the combined solution,

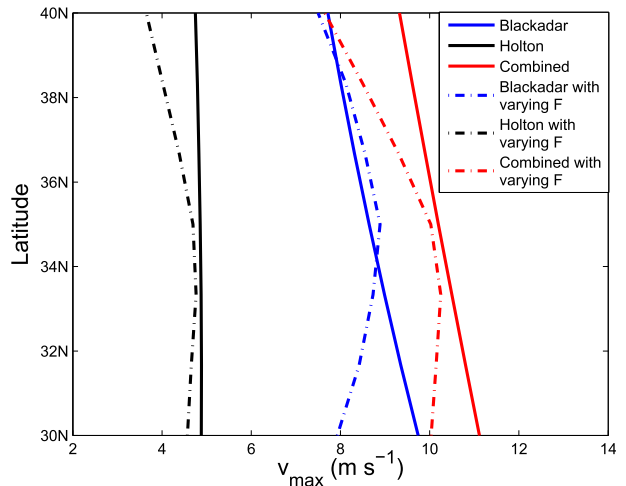


FIG. 9. Latitudinal variations of v_{max} (averaged along the x direction of the blue box in Fig. 6) for the Blackadar mechanism (blue), the Holton mechanism (black), and their combination (red). Solid and dashed lines indicate constant and latitudinally varying F , respectively.

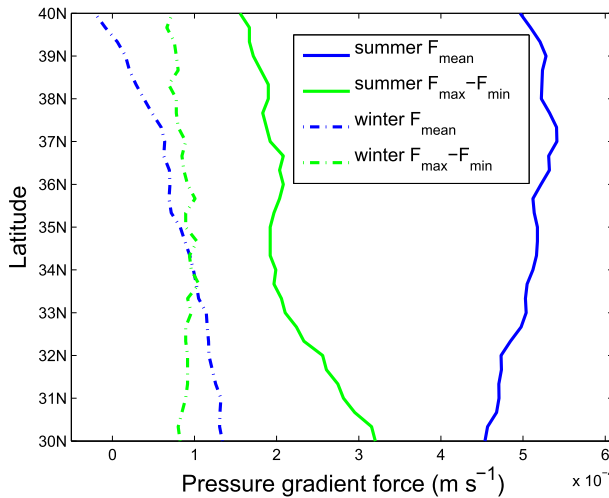


FIG. 10. Latitudinal variations of the mean pressure gradient force (blue; m s^{-2}) and the difference between the maximum and minimum pressure gradient forces in a day (green; m s^{-2}) from the NARR data (averaged along the x direction of the blue box in Fig. 6) during the summer (solid) and winter (dashed) seasons.

given by the dashed red lines in Figs. 8 and 9, are consistent with the NARR data (Fig. 7) and the results from J07.

The corresponding values of (\bar{F}, \hat{F}) for the winter season (December–February) are shown in Fig. 10 to be much weaker than the summer values; therefore, the present model, which has the weaker dimensional velocities $(u, v) = (\tilde{u}, \tilde{v})[(|\bar{F}| + |\hat{F}|)/\omega]$, is consistent with the observation that the southerly LLJ is most pronounced during the summer season (Whiteman et al. 1997; Mitchell et al. 1995; Song et al. 2005).

The present simple model suggests that the LLJ over the Great Plains has a diurnal variation with a maximum ($v \approx 10 \text{ m s}^{-1}$) around 0100 LST and is the result of the combination of the Holton mechanism ($v \approx 5 \text{ m s}^{-1}$, 2200 LST) and the Blackadar mechanism ($v \approx 8 \text{ m s}^{-1}$, 0300 LST). The Blackadar mechanism results in the latitudinal shift of the time of v_{max} , but the combined mechanism with varying \bar{F} and \hat{F} counteracts the degree of shift. The Blackadar mechanism also leads to a larger amplitude of the LLJ at lower latitudes, but varying \bar{F} and \hat{F} with latitude as observed gives a maximum amplitude near 34°N . Therefore, the observed amplitude and phase of the LLJ as a function of latitude can be reproduced in our simple model in which both Blackadar and Holton mechanisms are introduced with latitudinally varying \bar{F} and \hat{F} .

5. Summary

The inertial-oscillation theory proposed by Blackadar (1957) and diurnal heating over the sloping terrain

proposed by Holton (1967) are the two main theories for the LLJ over the Great Plains. To understand more precisely the role of each mechanism in the diurnally varying LLJ and its dependence on latitude, boundary layer friction, and the mean and diurnal pressure gradients, a simple analytical one-dimensional linear model is developed including both diurnal thermal forcing over sloping terrain and a diurnally varying friction coefficient.

Considering the significant difference of boundary layer friction between daytime and nighttime, the periodic solutions are similarly divided into daytime and nighttime intervals with conditions on the continuity of the velocity at the transitions: $U_1(\tau)$ is the daytime solution with large friction coefficient b_1 and $U_2(\tau)$ is the nighttime solution with small friction coefficient b_2 . With the analytical solutions of the present model, three problems are discussed.

- 1) The Holton mechanism (diurnal thermal forcing, time-independent friction coefficient): with increasing friction the jet speed maximum v_{max} decreases and shifts in time to between 1800 and 2300 LST, which is earlier than the observed maximum.
- 2) The Blackadar mechanism (constant thermal forcing, diurnally varying friction coefficient): v_{max} occurs earlier at high latitudes than at low latitudes because of the shorter inertial period. The magnitude and timing of v_{max} are sensitive to the daytime friction coefficient, whereas primarily its magnitude is sensitive to the nighttime friction coefficient.
- 3) The combined mechanisms (diurnal thermal forcing, diurnally varying friction coefficient): v_{max} occurs (~ 0100 LST) between the time obtained in the pure Holton mechanism (~ 2200 LST) and the time obtained in the pure Blackadar mechanism (~ 0300 LST); furthermore, its magnitude is larger than in either one individually and closer to the observed values.

The amplitude and phase of the LLJ as a function of latitude can be reproduced in the present model with latitudinally varying \bar{F} and \hat{F} . The maximum diurnal amplitude of the LLJ occurs around 34°N and is mainly due to the variation of \bar{F} and \hat{F} with latitude. The Blackadar mechanism leads to the latitudinal shift of the time of v_{max} , but the combination of the two mechanisms with varying \bar{F} and \hat{F} counteracts the degree of shift.

Blackadar (1957) suggested in his paper that the height of the maximum LLJ winds would be expected to rise overnight toward sunrise as the height of the nocturnal inversion rises. A 2-yr study (Mitchell et al. 1995) using wind profiler observations confirmed this (about 100–200-m height variations of the jet location). As our model is 1D, it cannot have this effect.

This simple analytical model is applied to explain the LLJ over the Great Plains in this study. In the future, features of LLJs over other regions of the world will be studied with this model. Du et al. (2012), using a wind profiler radar, found that the low-level jet in Shanghai (near the eastern coast of China) exhibits pronounced diurnal variations in the boundary layer. It is noted that the diurnal thermal contrast of coastal regions is similar to sloping terrain, so it will be interesting to study coastal jets with the present model. Furthermore, Pu and Dickinson (2014), using a two-dimensional (x - y), one-layer linear model, showed that diurnal oscillation of the LLJ over the Great Plains contributes to the diurnal phasing of the vertical motions (and thus to precipitation). Du et al. (2014), in an analysis using the Weather Research and Forecasting (WRF) Model to simulate the warm-season climatology of the LLJ in China, also suggested that the eastward propagation of precipitation east of the Tibetan Plateau (TP) is closely related to the diurnal variation of the LLJs. It will be of interest to see whether the simplified models proposed here and in Pu and Dickinson (2014) can describe the LLJ and its relation to the diurnal precipitation features in other geographical contexts.

Acknowledgments. This study is supported by the Chinese 973 Program 2013CB430104 and the Chinese National Science Foundation under Grants 40921160380 and 41330421. The authors gratefully acknowledge financial support from the China Scholarship Council. The authors are thankful to Peggy LeMone and Stan Trier for internal reviews, the three anonymous reviewers for their valuable comments, and Qinghong Zhang for fruitful discussions.

REFERENCES

- Banta, R. M., R. K. Newsom, J. K. Lundquist, Y. L. Pichugina, R. L. Coulter, and L. Mahrt, 2002: Nocturnal low-level jet characteristics over Kansas during CASES-99. *Bound.-Layer Meteor.*, **105**, 221–252, doi:10.1023/A:1019992330866.
- Blackadar, A. K., 1957: Boundary layer wind maxima and their significance for the growth of nocturnal inversions. *Bull. Amer. Meteor. Soc.*, **38**, 283–290.
- Bonner, W. D., 1968: Climatology of the low level jet. *Mon. Wea. Rev.*, **96**, 833–850, doi:10.1175/1520-0493(1968)096<0833:COTLLJ>2.0.CO;2.
- , and J. Paegle, 1970: Diurnal variations in boundary layer winds over the south-central United States in summer. *Mon. Wea. Rev.*, **98**, 735–744, doi:10.1175/1520-0493(1970)098<0735:DVIBLW>2.3.CO;2.
- Du, Y., Q. Zhang, Y. Yue, and Y. Yang, 2012: Characteristics of low-level jets in Shanghai during the 2008–2009 warm seasons as inferred from wind profiler radar data. *J. Meteor. Soc. Japan*, **90**, 891–903, doi:10.2151/jmsj.2012-603.
- , —, Y.-L. Chen, Y. Zhao, and X. Wang, 2014: Numerical simulations of spatial distributions and diurnal variations of low-level jets in China during early summer. *J. Climate*, **27**, 5748–5767, doi:10.1175/JCLI-D-13-00571.1.
- Haurwitz, B., 1947: Comments on the sea-breeze circulation. *J. Meteor.*, **4**, 1–8, doi:10.1175/1520-0469(1947)004<0001:COTSBC>2.0.CO;2.
- Holton, J. R., 1967: The diurnal boundary layer wind oscillation above sloping terrain. *Tellus*, **19A**, 199–205, doi:10.1111/j.2153-3490.1967.tb01473.x.
- Jiang, X., N. C. Lau, I. M. Held, and J. J. Ploshay, 2007: Mechanisms of the Great Plains low-level jet as simulated in an AGCM. *J. Atmos. Sci.*, **64**, 532–547, doi:10.1175/JAS3847.1.
- Mesinger, F., and Coauthors, 2006: North American Regional Reanalysis. *Bull. Amer. Meteor. Soc.*, **87**, 343–360, doi:10.1175/BAMS-87-3-343.
- Mitchell, M. J., R. W. Arritt, and K. Labas, 1995: A climatology of the warm season Great Plains low-level jet using wind profiler observations. *Wea. Forecasting*, **10**, 576–591, doi:10.1175/1520-0434(1995)010<0576:ACOTWS>2.0.CO;2.
- Paegle, J., and G. E. Rasch, 1973: Three-dimensional characteristics of diurnally varying boundary-layer flows. *Mon. Wea. Rev.*, **101**, 746–756, doi:10.1175/1520-0493(1973)101<0746:TCODVB>2.3.CO;2.
- Parish, T. R., and L. D. Oolman, 2010: On the role of sloping terrain in the forcing of the Great Plains low-level jet. *J. Atmos. Sci.*, **67**, 2690–2699, doi:10.1175/2010JAS3368.1.
- Pu, B., and R. E. Dickinson, 2014: Diurnal spatial variability of Great Plains summer precipitation related to the dynamics of the low-level jet. *J. Atmos. Sci.*, **71**, 1807–1817, doi:10.1175/JAS-D-13-0243.1.
- Rife, D. L., J. O. Pinto, A. J. Monaghan, C. A. Davis, and J. R. Hannan, 2010: Global distribution and characteristics of diurnally varying low-level jets. *J. Climate*, **23**, 5041–5064, doi:10.1175/2010JCLI3514.1.
- Schmidt, F. H., 1947: An elementary theory of the land- and sea-breeze circulation. *J. Meteor.*, **4**, 9–20, doi:10.1175/1520-0469(1947)004<0009:AETOTL>2.0.CO;2.
- Shapiro, A., and E. Fedorovich, 2009: Nocturnal low-level jet over a shallow slope. *Acta Geophys.*, **57**, 950–980, doi:10.2478/s11600-009-0026-5.
- , and —, 2010: Analytical description of a nocturnal low-level jet. *Quart. J. Roy. Meteor. Soc.*, **136**, 1255–1262, doi:10.1002/qj.628.
- Song, J., K. Liao, R. L. Coulter, and B. M. Lesht, 2005: Climatology of the low-level jet at the Southern Great Plains Atmospheric Boundary Layer Experiments site. *J. Appl. Meteor.*, **44**, 1593–1606, doi:10.1175/JAM2294.1.
- Van de Wiel, B. J. H., A. Moene, G. Steeneveld, P. Baas, F. Bosveld, and A. Holtslag, 2010: A conceptual view on inertial oscillations and nocturnal low-level jets. *J. Atmos. Sci.*, **67**, 2679–2689, doi:10.1175/2010JAS3289.1.
- Whiteman, C. D., X. Bian, and S. Zhong, 1997: Low-level jet climatology from enhanced rawinsonde observations at a site in the southern Great Plains. *J. Appl. Meteor.*, **36**, 1363–1376, doi:10.1175/1520-0450(1997)036<1363:LLJCFE>2.0.CO;2.
- Zhong, S., J. D. Fast, and X. Bian, 1996: A case study of the Great Plains low-level jet using wind profiler network data and a high-resolution mesoscale model. *Mon. Wea. Rev.*, **124**, 785–806, doi:10.1175/1520-0493(1996)124<0785:ACSOTG>2.0.CO;2.